Fluorescence-free First Hyperpolarizability Values of Fluorescent Proteins and Channel Rhodopsins

Evelien de Meulenaere, Yovan de Coene, Isabelle Russier-Antoine, Louis Vanpraet, Chris van den Haute, Karin Thevissen, Veerle Baekelandt, Carmen Bartic, Johan Hofkens, Pierre-François Brevet, et al.

Fluorescence-free First Hyperpolarizability Values of Fluorescent Proteins and Channel Rhodopsins

Evelien De Meulenaere[1,2], Yovan de Coene[1], Isabelle Russier-Antoine[3], Louis Vanpraet[1], Chris Van den Haute[4], Karin Thevissen[2], Veerle Baekelandt[4], Carmen Bartic[5], Johan Hofkens[1], Pierre-François Brevet[3*], Koen Clays[1]

[1] Department of Chemistry, University of Leuven, Celestijnenlaan 200D, B-3001 Leuven, Belgium

[2] Department of Microbial and Molecular Systems, University of Leuven, Kasteelpark Arenberg 20, B-3001 Leuven

[3] Institut Lumière Matière, Université de Lyon, UMR CNRS 5306, Université Claude Bernard Lyon 1, 10 Rue Ada Byron, F-69622 Villeurbanne cedex, France

[4] Department of Neurosciences, University of Leuven, Herestraat 49, B-3000 Leuven, Belgium

[5] Department of Physics and Astronomy, University of Leuven, Celestijnenlaan 200D, B-3001 Leuven, Belgium

* Corresponding author : Pierre-François Brevet, pfbrevet@univ-lyon1.fr

Abstract

The fluorescence-free measurement of molecular second-order nonlinear optical properties (*i.e.* the first hyperpolarizability β) in solution for a set of fluorescent proteins and channel rhodopsins is reported. Because removing the fluorescence contribution is critical in providing accurate values for this nonlinear optical property, especially for the fluorescent proteins, we use and critically compare two different approaches to correct hyper Rayleigh scattering from the multiphoton fluorescence contribution. On the one hand, we use the frequency domain where the delayed fluorescence contribution is separated from the instantaneous hyper-Rayleigh scattering contribution through amplitude modulation and on the other hand we use the spectral domain where the broadband fluorescence spectrum is subtracted from the narrower hyper Rayleigh scattering line. The two methods, discussed in terms of their efficiency for routine measurements, yield similar first hyperpolarizability values, therefore establishing the robustness of the two approaches to correct for the fluorescence. From the data reported, the previously observed trend where more red-shifted fluorescent proteins have larger hyperpolarizability values because of their longer conjugated chromophore is unambiguously confirmed. For the channel rhodopsins, it is shown that despite their obligate dimeric and fairly symmetric nature, large first hyperpolarizabilities are measured, pointing to their potential use for second-harmonic imaging and membrane potential measurements in nonlinear optogenetics.

Keywords

Fluorescent proteins, opsins, channel rhodopsins, fluorescence-free hyperpolarizability, hyper-Rayleigh scattering

List of abbreviations

AA: Amino acid

AM: Amplitude modulation

bR: BacterioRhodopsin

CCD: Charged coupled device

ChR: Channel rhodopsin

DDM: n-dodecyl beta-D-maltoside

EFISHG: Electric-field-induced second-harmonic generation

eYFP: Enhanced Yellow Fluorescent Protein

FP: Fluorescent proteins

GaAsP: Gallium Arsenide Phosphide

GFP: Green Fluorescent Protein

HRS: Hyper-Rayleigh scattering

MPF: Multiphoton fluorescence

NIR: Near-infrared

PMT: Photomultiplier tube

PRSB: Protonated retinal Schiff base

RF: radio frequency

SHG: Second-harmonic generation

SHIM: Second-harmonic imaging

Introduction

Fluorescent proteins (FPs) are omnipresent in biomedical research nowadays, mostly because of their genetically encoded nature, enabling researchers to uniquely and covalently label one specific protein with one specific color. An ever increasing rainbow of FPs emitting from the blue to the near-infrared [1, 2], combined with multiplexing strategies based on small band pass filters or even deconvolution methods, allows for the generation of multi-color images to elucidate complex processes involving multiple proteins [3-5]. Up to now, multiphoton fluorescence (MPF) from these protein markers has been used in cellular nonlinear optical microscopy and spectroscopy. Nonlinear imaging has the advantage over linear imaging to be associated with excitation in the near-infrared (NIR). The advantages include less background emission, less scattering and therefore deeper penetration and reduced out-of-focus phototoxicity or photobleaching. A higher resolution, especially in the depth profile, also results in this inherent confocal imaging method. On the downside however, multiphoton excitation requires a large number of photons focused in space and time, translating in the necessary use of focused pulsed lasers to attain the required peak intensities [6].

Besides their application in fluorescence imaging, FPs have been used for second-harmonic generation (SHG) imaging, a nonlinear optical process where two photons at a fundamental frequency are converted into a single photon at the harmonic frequency. As a standard example beyond dyes and SHG nanoprobes based on crystalline materials [7], one may cite the Green Fluorescent Protein (GFP) that has been used to image the membrane potential by SHG [8-11]. Despite being designed and engineered for a different optical process, namely linear or nonlinear fluorescence, some of these proteins have been shown to exhibit an appreciable second-order optical nonlinearity [12-15]. However, reporting their efficiency for SHG is not a simple task as FPs have the challenge of being charged species exhibiting strong MPF. Charged species are not amenable to electric-field-induced second-harmonic generation (EFISHG), a standard characterization method yielding large SHG signals [16]. Even at their iso-electric point, the pH at which a protein carries no net charge, the resulting charge distribution over the protein will determine the protein alignment rather than the chromophore orientation in the interior of the protein barrel, a requisite in EFISHG measurements [17].

In addition to FPs, also chromoproteins are of interest for second-order nonlinear optical imaging applications. Chromoproteins are proteins with an absorption peak in the visible range but with no or very weak fluorescence. An example that is gaining increasing interest is the family of opsins. Opsins are light-sensitive proteins that commonly have a small molecule bound to them that acts as a chromophore, *e.g.* retinal, bilin or a flavin. Opsins are used in optogenetics for the optical excitation of nerve cells *in vitro* and in live animals using blue light for instance [18, 19]. Currently, reading out of the response is performed with invasive methods like patch-clamp for which only single cells can be targeted and must be perforated with needles. A combination with second-harmonic imaging would open up opportunities to optically, and noninvasively, read out the response of multiple neurons simultaneously, without unintentionally exciting the neurons. Opsins have been shown to exhibit second-order nonlinear optical properties [20]. Since the wavelength for SHG can be selected from a wide range of available pulsed laser wavelengths, nonlinear optogenetics can be envisaged for noninvasive monitoring of neuronal activity while avoiding wavelengths activating the opsins and exciting the nerve cell. Therefore, from the growing number of applications of nonlinear optics in biophysical and biomedical research using proteins or opsins, *e.g.* second-harmonic imaging (SHIM), membrane potential measurements or nonlinear optogenetics, the choice of a genetically encoded contrasting agent is essential. A large variety of FPs and opsins is available to choose from and it has become important to be able to rapidly select the most efficient ones. There is thus a need for a time-effective, yet efficient technique to subtract the MPF contribution from the total signal at the SHG wavelength, to arrive at the true and accurate values for the first hyperpolarizability. As a result, hyper-Rayleigh scattering (HRS) has become the standard method to determine the first hyperpolarizability value of molecules and non-fluorescent proteins [20] and, to some extent, some fluorescent proteins [12-15].

In this work, we have further extended our palette of FPs in the yellow (with Venus) to the blue (with Sirius) and to the near-infrared (with NirFP) [21-23]. We have also identified a number of channel rhodopsin (ChR) mutants that are currently being used in optogenetics for their improved cation conductivity and/or light sensitivity. C1C2 is a chimera of two naturally occurring ChRs (ChR1 and ChR2) [24]. A mutation in the highly conserved gating residue E129 has a large effect, thereby turning the ChR into a neuronal action potential inhibitor [25]. In the C1C2 E129K mutant, glutamate (E), a polar, acidic and thus negatively

charged amino acid (AA) residue, is replaced by lysine (K), a polar, yet basic and thus positively charged AA residue. Since the negative E129 has a direct interaction with the protonated retinal Schiff base (PRSB) in ChR, a change in AA is expected to have an impact on several optical properties [26]. ChR2 H134R is also a functional mutant of ChR2, inducing larger photocurrents than the wild-type ChR2 [25] whereas ChR2 C128T is a step-function opsin, enabling bi-stable modulation with photocurrents precisely initiated and terminated by pulses of light with different wavelengths [28, 29]. ChR2 C128T has its cysteine residue in position 128 replaced by a threonine in the wild type ChR2. This mutant is specifically selected because of its slow switching properties to ensure that the nonlinear optical characterization is not based on both the inactive (*all-trans*-retinal) and the activated (11-*cis*-retinal) conformations. We compare the results with the published value for bacterioRhodopsin [20].

Principle of the fluorescence deconvolution methods

Because the removal of the MPF is critical and a potential source of systematic errors in the first hyperpolarizability values reported, a careful deconvolution study is employed where two methods are compared, one performed in the time [30] or equivalently, in the frequency domain [31-33], and the other in the spectral domain [34-40]. In the frequency domain, the HRS response is recorded as a function of an amplitude modulation (AM) frequency. It is then possible to distinguish between the slow MPF response and the fast HRS response. The mathematical expressions of the Fourier transform yield an amplitude and a phase, both function of the AM frequency. They can be experimentally determined and their simultaneous fitting as functions of AM frequency provide multi-exponential fluorescence lifetimes and first hyperpolarizabilities with high precision and excellent accuracy. Experimentally, this approach takes advantage of the availability of high-repetition rate (about 100 MHz) femtosecond (about 100-200 fs) laser sources such as Titanium-sapphire laser oscillators with their inherent ultra-high harmonic content in the frequency domain up to the inverse of 100 fs, *i.e.* 10^{13} Hz, as derived from the strong “harmonic distortion” of the ultra-short femtosecond pulse. There is no need to additionally apply an external amplitude modulation. All the harmonics of the fundamental repetition frequency of 100 MHz are present up to 10 THz. The limiting factor is the response time of the photodetector typically restricting the frequency bandwidth of the instrument to a few GHz. The approach is intuitively clearer in the time domain where the

incident short pulse is causing the immediate HRS while the MPF is time-delayed because of the finite lifetime of the real excited states involved. By selecting an appropriate early and short time gate, it is possible to largely exclude the later fluorescence from contributing to the immediate nonlinear scattering (HRS) signal [30]. Because the fluorescence lifetime is typically in the few nanoseconds range, the use of the historical nanosecond pulses from Q-switched Neodymium-YAG lasers is excluded for this approach. In the spectral domain, it is also intuitively clear that a continuous MPF spectrum can easily be discerned from a discrete SHG response centered around the second-harmonic wavelength. This approach has originally been introduced for the early nanosecond pulsed lasers with a wavelength scanning spectrometer [34]. Fitting the total response to the sum of a number of broad fluorescence background(s) and a narrow HRS peak as a function of signal emission wavelength allows for discerning between HRS and MPF. The recent availability of very sensitive cooled diode arrays for detecting the wavelength dependence at once has solved the earlier time-consuming problem of scanning the detection wavelength.

From the nature of hyper-Rayleigh scattering, *i.e.* an incoherent second-order nonlinear scattering in all directions from an isotropic solution of scatterers, it follows that the photon efficiency is extremely low. For that reason, the use of pulsed lasers and spatial focusing are intrinsically necessary to obtain the required peak intensity for any HRS to be observed. Therefore, the excitation part of experimental setups for HRS is highly identical, independent of the implemented deconvolution technique whether in the time or spectral domain. Nowadays, the pulsed laser of choice is the tunable mode-locked femtosecond Ti:sapphire laser emitting at a fundamental wavelength around 800 nm in pulses with a duration of about 100 to 200 femtoseconds at a repetition rate of about 80 to 100 MHz although new sources are appearing on the market. After passing through a low-pass filter to remove any unwanted harmonic light generated prior to the cell, the fundamental beam of about 1 W is focused in a spectrophotometric cell containing the aqueous solutions. The HRS light is collected at an angle of 90° from the incident direction by an efficient condensing system [32].

From here on, the different deconvolution schemes for discriminating between HRS and MPF imply different experimental approaches for time domain *vs.* wavelength domain measurement techniques. For the

wavelength domain approach, the HRS signal is separated from the excitation light by a high-pass filter and sent through a spectrometer that is scanned over the second harmonic wavelength, typically around 400 nm for a Ti:sapphire laser, either over a broadband 350 to 600 nm range to observe the full MPF spectrum or more typically from 390 to 410 nm to concentrate on the narrow HRS peak on top of the broad MPF background. The HRS or MPF photons can then be detected as a function of wavelength by a photomultiplier tube (PMT) working in the single photon counting regime. Alternatively, a sensitive linear diode array or charged coupled device (CCD) camera can be used to detect the dispersed wavelength region of interest at once. As the two contributions to the overall signal, HRS and MPF are two incoherent processes that simply add up. Any broadband MPF contribution can thus be rejected by curve fitting of the resulting spectrum to a simple sum of Gaussians and subtracting the broadband MPF background from the total spectrum. The top part of Figure 1 shows a typical narrow HRS band on top of the MPF within the typical wavelength frame of 390 - 410 nm, for different concentrations of the FP named Venus. The lower panel shows the HRS intensity normalized to the buffer solution intensity.

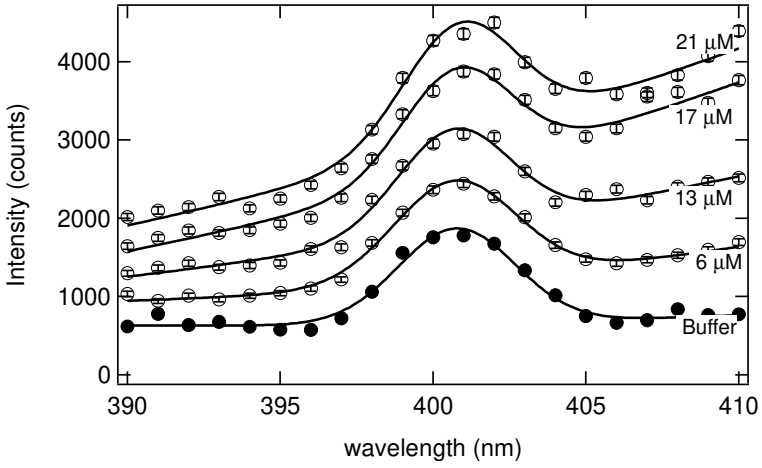

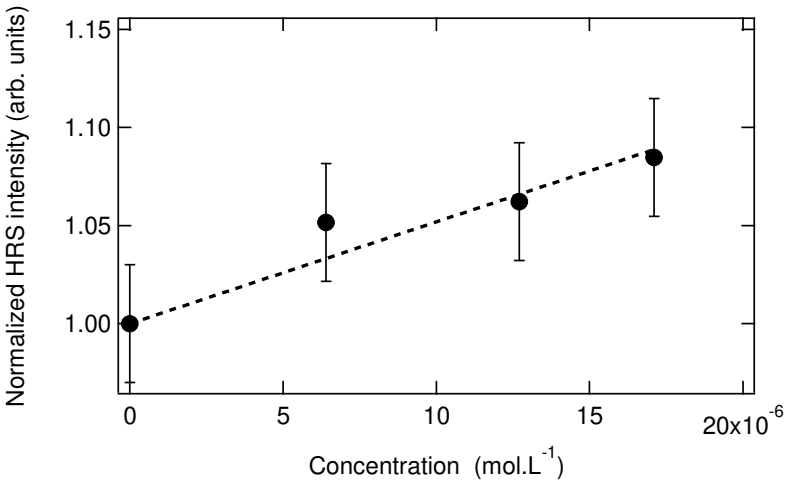

Figure 1. (Top panel) HRS intensity versus emission wavelength for solutions of Venus (FP) at different concentrations (empty circles) indicated on the panel right side and for the buffer only (filled circles). Line: fit to a Gaussian function superposed on a broadband multi-gaussian fit for the MPF background. (Bottom panel) Plot and linear fit of the HRS intensity normalized to the buffer HRS intensity as a function of concentration for Venus protein.

This implementation of the background MPF spectral subtraction is rather efficient as can be appreciated from Figure 2 that exemplifies the relative contributions of the HRS contribution as a small shoulder on an overwhelming MPF spectrum for the case of the ultramarine emitting FP Sirius [41] or the much stronger but red shifted FP DsRed. It is clear that without properly accounting for the MPF contributions to the total signal, huge overestimations of the hyperpolarizability (β) values will result.

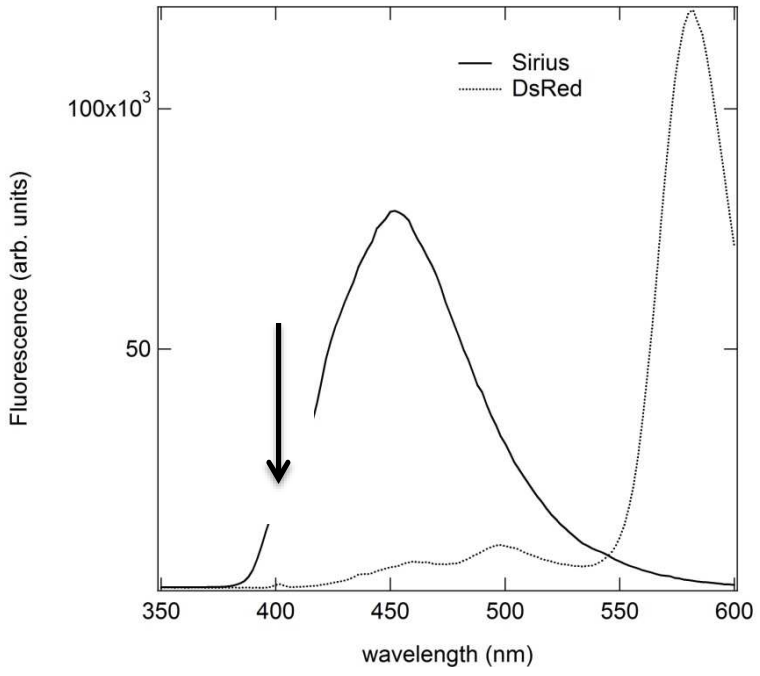

Figure 2. MPF spectra for the ultramarine emitting FP Sirius and the red emitting DsRed FP as a function of emission wavelength for an excitation wavelength of 800 nm. The MPF contribution at 400 nm is enormous for Sirius but appears almost negligible in DsRed. The arrow indicates the position of the HRS line.

In the frequency domain approach, after the condensing system described earlier, the scattered light is first sent to an interference filter matching the SHG wavelength to eliminate all MPF that is not coinciding with that wavelength. To eliminate the contribution of MPF that passes through the interference filter at that wavelength, an AM scheme is applied. For successively higher AM frequencies, the amplitude of the slower, delayed MPF contribution is lowered by active demodulation, while only the instantaneous HRS retains its amplitude, resulting in a lowering of the apparent hyperpolarizability (β) value for increasing frequencies, as exemplified in Figure 3, left panel. The phase of the signal also grows to a maximum, see Figure 3 right panel, as a result of first an increasing phase for increasing frequency due to the delayed MPF contribution and later a decreasing phase as all the MPF becomes demodulated and the high frequency signal is comprised of only the instantaneous HRS. Global fitting of both the apparent value and the phase towards the high-frequency limiting β value, the MPF contribution at low frequency and a fluorescence lifetime (or multiple lifetimes and relative amplitudes if required) results in the accurate MPF free β value. Experimental details of the optical set-up and the high-frequency electronics for the demodulation have been previously published [32]. These two methods have been implemented here in order to design an HRS set-up providing a simple and efficient way to provide fluorescence-free first hyperpolarizabilities. For frequency resolved experiments, Crystal Violet dissolved in Methanol was used as an external reference whereas in spectrally resolved experiments, the buffer solution was used as the internal reference. In the latter case, the buffer solution was itself externally referenced to neat water [30, 33].

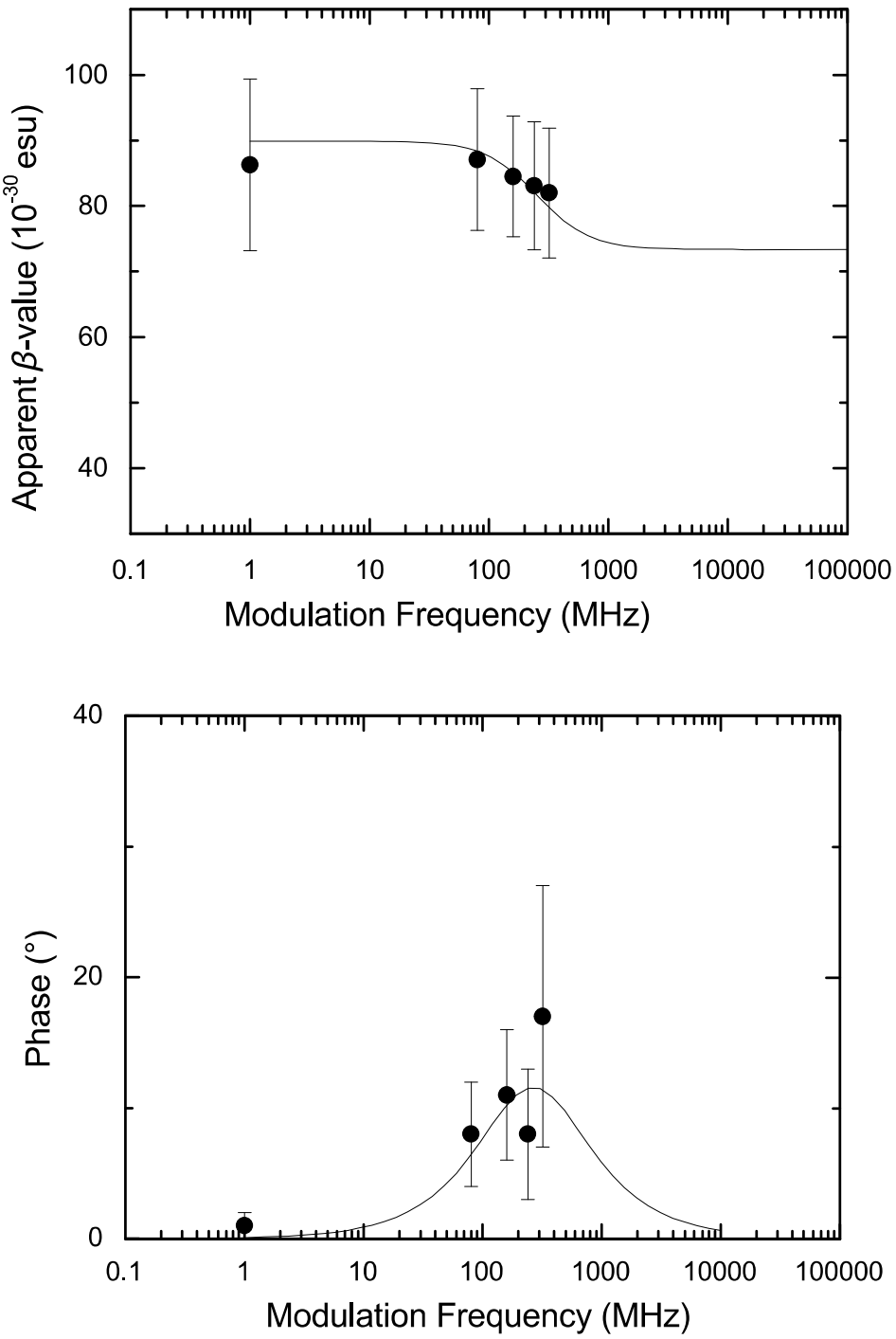

Figure 3. Top panel shows the decreasing apparent hyperpolarizability at 800 nm with increasing amplitude modulation frequency, right panel shows the phase as a function of amplitude modulation frequency for DsRed. Continuous lines are fits to single fluorescence lifetime model.

Preparation and purification

All FPs were recombinantly expressed in *Escherichia coli* (BL21 star™ (DE3), Invitrogen) which was harvested by centrifugation at 5,000 rcf for 20 min at 4 °C. Bacteria were lysed by incubating with lysozyme (from chicken egg white, Sigma Aldrich) in a shaking incubator at 37°C for 30 min, and an additional 30 min with Benzonase® (Sigma Aldrich), followed by sonication of the cells on ice. The resulting lysate was centrifuged at 25,000 rcf for 15 min at 4 °C. The supernatant was loaded onto a 5 mL Ni-NTA HisTrap column (GE Healthcare) using an Äkta Purifier FPLC system (Amersham Biosciences) for purification using affinity chromatography for the His_6 tag encoded in the FP plasmids and then followed by gel filtration over a Superdex 200 size exclusion column. All samples were concentrated using Vivaspin concentrators (VivaScience, molecular weight cutoff 10 kDa) and dialyzed in a 20 mM Na-phosphate buffer (pH 7.4) with 300 mM NaCl.

The Channel Rhodopsin (ChR) mutants were expressed in *Pichia pastoris* X33 using plasmid pPICZαA, based on the instructions in the manual of the EasySelect™ *Pichia* Expression Kit (Invitrogen). Expression was induced by switching the cultures to a growth medium containing 2.5% methanol. At this step of the cultivation, *all-trans* retinal was added to the medium at a final concentration of 5 µM. Cells were harvested at room temperature at 1,500 × g for 15 min and lysis was performed with a French Press. The membrane fraction was isolated by centrifugation of the lysate at 30,000 × g 15 min and 4 °C, followed by ultracentrifugation of the supernatant at 100,000 × g for 1 hour at 4 °C. The membrane fraction was homogenized using a glass potter tube and was solubilized overnight using n-dodecyl beta-D-maltoside (DDM) detergent. After solubilization, the sample was cleared by centrifugation at 100,000 × g for 1 hour at 4°C to remove all non-solubilized membrane. Just like the FP, each ChR mutant is tagged with a His_6 tag and was purified from the lysate on a Ni-NTA column and Superdex 200 size exclusion column using an Äkta Purifier FPLC system (Amersham Biosciences). The final sample was re-suspended in the FP buffer described above with 0.1% DDM to keep the membrane protein in solution.

First hyperpolarizability (β) measurements

The first hyperpolarizability values at 800 nm for the selection of FPs and opsins measured in this work are provided in Table 1. It is clear that the applied treatment of the fluorescence at the second harmonic wavelength, either in the spectral domain by subtracting the fluorescence background from the total signal, or in the frequency domain by taking the high-frequency value of extrapolated estimate, is appropriately correcting for more and less significant contributions of MPF in the signal and results in essentially the same value within estimated statistical error.

Table 1. First hyperpolarizability of the FPs and one opsins : comparison of the dynamic (at 800 nm) first hyperpolarizability values $\beta_{HRS,800nm}$ for different proteins (first column) as obtained from the spectral (second column) and from the frequency domain technique (third and fourth column), resulting static first hyperpolarizability values $\beta_{HRS,o}$ based on the two-level model (fifth column) with resonance wavelength at maximum absorption $\lambda_{max,abs}$ (sixth column) and wavelength of maximal emission for fluorescent proteins $\lambda_{max,em}$ (seventh column). All hyperpolarizabilities are reported in units of 10^{-30} esu and wavelengths in nm.

$\beta_{HRS,800nm}$ (10^{-30} esu) Protein sample	spectral domain HRS	frequency domain HRS	frequency domain HRS literature values	$\beta_{HRS,o}$	$\lambda_{max,abs}$	$\lambda_{max,em}$
Sirius	158±11			27±2	355	424
eGFP	115±5		107±17[a]	33±5[a]	488	507
Venus	45±5			24±4	515	528
SHardonnay			74±5[c]	28±2[c]	511	524
eYFP			37±4[a,c]	14±2 [a,c]	514	527
zFP538			90±5[c]	38±2[c]	528	538
DsRed	63±1	62±10	81±8[a]	39±4[a]	558	583
mStrawberry			104±8[b]	54±4[b]	575	596
mCherry	122±2	123±9	134±16[b]	71±9[b]	587	610
NirFP	80±3	107±10		44±2; 59±6	605	670
ChR C128T	166±4	173±21		41±1; 43±5	470	
bacterioRhodopsin			220[d]	110	570	

[a] from reference [13], [b] from reference [14], [c] from reference [15], [d] from reference [20]

The results of the incoherent nonlinear scattering experiments are reported in terms of the orientation-averaged β_{HRS}. From the nature of the monomeric FPs with a single dipolar chromophore derived from an autocatalytic, post-translational oxidation of 3 amino acids, *e.g.* threonine-65, tyrosine-66 and glycine-67 in eGFP, the enhanced Green Fluorescent Protein, or glutamine-66, tyrosine-67 and glycine-68 in DsRed, it can be conjectured that the major first hyperpolarizability tensor component is the diagonal β_{zzz} tensor element. This allows the estimation of the value for this unique tensor element as square root of 6/35 times larger than the value for β_{HRS}.

Table 2. First hyperpolarizability of the Channel Rhodopsins: comparison of the dynamic (at 1064 nm) first hyperpolarizability values $\beta_{HRS,1064nm}$ for different ChRs as obtained from the spectral domain technique (second column), resulting static first hyperpolarizability values $\beta_{HRS,o}$ based on the two-level model with resonance wavelength at maximum absorption $\lambda_{max,abs}$ (third and fourth columns). All hyperpolarizabilities are reported in units of 10^{-30} esu and wavelengths in nm.

$\beta_{HRS,1064nm}$ (10^{-30} esu) ChR sample	spectral domain HRS	$\beta_{HRS,o}$	$\lambda_{max,abs}$
C1C2	500±20	90±4	470
C1C2 E129K	1000±20	150±3	480
ChR2 H134R	440±20	80±4	470
ChR2 C128T	600±10	105±2	470
bacterioRhodopsin	460±10[a]	49±1	570

[a] from reference [20]

When the FP is not in a monomeric form, it is more difficult to interpret the β_{HRS} result in terms of tensor components. For DsRed, which is known to be in a tetrameric form, an HRS depolarization ratio of 2.6±0.2 is experimentally observed for the fundamental wavelength of 800 nm, see Figure 4. This value has to be compared with the limiting values of 1.5 observed for octupolar molecules and 5 for molecules with a one-dimensional push-pull character with a unique β_{zzz} tensor component [42-44]. A very similar value of 2.7±0.1 is observed for the depolarization ratio of the C128T ChR2. Such a value is in good agreement with a non-centrosymmetric arrangement of the 2 retinal moieties in the dimer.

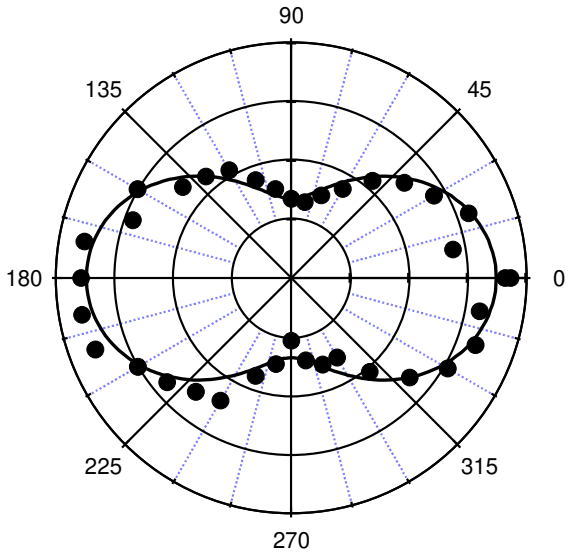

Figure 4. Polar plot of the HRS intensity (corrected by subtraction of the broadband MPF contribution) as a function of the angle of polarization of the fundamental beam at 800 nm for a 26×10^{-6} mol.L^{-1} concentration of DsRed protein. (Circles) experimental data, (Solid) adjusted curve revealing an HRS depolarization ratio of 2.6±0.2 for DsRed.

For the ultramarine fluorescent protein Sirius, one of the FPs with the most blue shifted emission maximum at 424 nm, in the immediate vicinity of the SHG wavelength of 400 nm for our HRS experiments, see Figure 2, we determine a rather precise value for the fluorescence-free first hyperpolarizability of $(158 \pm 11) \times 10^{-30}$ esu due to the simultaneous inherent proximity of the electronic resonance at a maximal absorption wavelength of 355 nm enabling a rather strong two-photon resonant enhancement. For the yellow-emitting FP Venus, an FP derived from the enhanced Yellow Fluorescent Protein (eYFP) with a maximal absorption wavelength at 515 nm and a fluorescence emission centered around 528 nm, the HRS response is spectrally much better separated from the red-shifted fluorescence but the hyperpolarizability value is much less resonantly enhanced at a fundamental wavelength of 800 nm.

At first sight, the values for the first hyperpolarizability of the proteins are all rather similar after correcting for the different degree of two-photon resonance enhancement with the undamped simple two-level model, see Table 1 static $\beta_{HRS,o}$ entries, fifth column. It has been shown that the remaining differences sometimes cannot be attributed to different chromophores but that a rationale for the variation in static $\beta_{HRS,o}$ value among different FPs has to invoke interactions with the chromophore surrounding in the protein matrix. A case in point is the low value for eYFP which has exactly the same chromophore moiety as eGFP which has been attributed to an overall centrosymmetry for the chromophore coupled to its surrounding. Based on a detailed understanding of this surrounding as derived from crystal structure if available, a point mutation can even be designed and executed to improve the $\beta_{HRS,o}$ value as has been exemplified and corroborated through quantum chemical calculations in SHardonnay [15].

It would go beyond the scope of this work to try to rationalize all the dynamic $\beta_{HRS,800nm}$ and static $\beta_{HRS,o}$ hyperpolarizability values in terms of the detailed chromophore structure and protein environment. We can underpin, however, two general observations: (i) larger dynamic $\beta_{HRS,800nm}$ values for blue emitting FPs (*e.g.*

Sirius) because of the stronger resonance enhancement with the absorption in the blue, yet (ii) larger static $\beta_{HRS,o}$ values for the FPs emitting towards the red end of the spectrum (*e.g.* mCherry). The first general observation underlines the importance of developing FPs and nonlinear optical contrast agents with a large Stokes shift to make use of resonance enhancement outside the emission spectrum, especially in conjunction with the use of the omnipresent Titanium-sapphire laser as the premier femtosecond laser pulsed source and its laser line around 800 nm, which is right in the middle of the first NIR biological window, where light of the wavelengths between 700 and 900 nm is less absorbed by biological tissue [45]. A change of laser to longer wavelengths, say towards the NIR-II biological window (1000 - 1350 nm), would only shift the required molecular engineering design towards the longer wavelengths [46]. In the furthest red-shifted options of this, the second-harmonic wavelength would now also be in the NIR-I window. Large hyperpolarizabilities, and hence strong nonlinear imaging signals and high membrane potential sensitivity is then offered by blue absorbing FPs with their absorption band around 400 nm but the fluorescence emission would still be ideally in the much longer wavelength region. The concomitant approach towards longer wavelength emission offered by FPs with the extension of the conjugated fluorescent chromophore as elaborated in mCherry results in stronger nonlinear optical properties that still show a large β after the correction for weaker resonance enhancement, as underpinned by the second general observation. The result for NirFP, however, is not in line with the latter observation. This is explained by the different chromophore structure in NirFP when compared to all other FPs. The chromophore is derived from phytochrome, via symmetric heme oxidation of the also symmetric biliverdin [47]. While this biliverdin has a longer conjugation pathway resulting in the longer wavelengths for absorption and fluorescence, its higher symmetry with respect to the chromophores of the GFP family results in the lower second-order nonlinear response.

The ChRs are not FPs, and as such, can also be termed chromoproteins, as they have a non-fluorescent chromophore inside their protein structure. We have been interested in the first hyperpolarizability of bacterioRhodopsin (bR) earlier [20] and have recently reported the wavelength dependence of its first hyperpolarizability [38]. Even though in both bR and the ChRs, the retinal protonated Schiff base linked to a lysine is the actual chromophore, a relatively large shift in the absorption spectrum is observed between bR

and the ChRs. This means that the electronic properties of the chromophore are influenced by a change in the protein environment. Another significant difference is the monomeric nature for bR that is ensured by solubilizing with Triton X-100 [20, 27], in contrast to the obligate dimeric nature of the ChRs in their buffer. For a second-order nonlinear optical property, the orientational symmetry of the two retinal chromophores with respect to each other has to be considered. The bR before solubilization had been shown to be a trimer with octopolar threefold symmetry [20]. From the non-zero value for the first hyperpolarizability of all ChRs, it is clear that the two retinals in the ChR dimers are not centrosymmetric with respect to each other. With a good reference model for the monomer, it would be possible to arrive at an estimate for the opening angle and compare this value with crystal structure data [21, 22]. However, neither the PRSB itself nor the bR is a good model for the monomer in the ChRs as can be appreciated from the difference in resonance wavelength, pointing to the abovementioned electronic disturbance by the protein environment. Nevertheless, the sizeable values for the first hyperpolarizability of the selected ChRs show their potential for SHIM in neurons and for membrane potential measurements in optogenetics. The more red absorbing bR exhibits a larger first hyperpolarizability, both in its dynamic and static values, although the difference is smaller in the dynamic value because of the smaller resonance enhancement effect for bR in agreement with the earlier observation of larger hyperpolarizabilities for more red absorbing fluorescent proteins.

Table 3 gives an idea about the possible variation in the obtained first hyperpolarizability values for a particular FP, namely eGFP, for different samples. The differences can be related to small and non-systematic differences in buffer composition, for instance salt concentration, nature or charge and concentration of the buffering compound and especially pH. It should be appreciated that a protein in a buffer is much more complex and allows for much more degrees of freedom and hence, differences in results, than a single pure, commercially available and stable “small molecule” type compound in a simple solvent, *e.g. para*-nitroaniline in methanol. For eGFP in particular, it is known that the linear optical properties of the chromophore are sensitive to changes in pH [48]. However, the corresponding pH changes are small and we have therefore used the linear absorption spectra as indicators instead of a measure.

Table 3. Comparison of the variation in hyperpolarizability value between samples for fluorescent protein eGFP in slightly different buffers as obtained from the spectral domain technique (second column) and hyperpolarizability value obtained from the frequency domain technique (third column). All hyperpolarizabilities reported in units of 10^{-30} esu.

$\beta_{HRS,800nm}$ (10^{-30} esu) eGFP sample number	spectral domain HRS	frequency domain HRS
eGFP1	115±5	
eGFP2	92±10	
eGFP3	130±4	
eGFP phosphate buffer pH 7.3		107±17[a]

[a] from reference [13]

The chromophore exists in equilibrium between its protonated and deprotonated forms. The deprotonated form absorbs around 488 nm and emits around 507 nm while the protonated chromophore absorbs near 400 nm and is dark. Protonating the chromophore is lowering the photo-induced charge transfer from the phenolate residue of Tyr66 to the imidazolone moiety resulting from the oxidation, *i.e.* dehydrogenation, of the Gly65, Tyr66 and Gly67 residues. It is this charge transfer that is responsible for the linear as well as the nonlinear optical properties of the protein. A large transfer such as in the deprotonated state showing a longer wavelength absorption at 488 nm is related to a large first hyperpolarizability while a smaller charge transfer results in a shorter wavelength absorption at 400 nm, very small fluorescence efficiency (observed as a dark state) and the smaller first hyperpolarizability value. From linear absorption spectra, see Figure 5, we can learn that one of the samples (eGFP2) has a larger fraction of its chromophores in the dark state, leading to a resulting $\beta_{HRS,800nm}$ of 92x10^{-30} esu, a value smaller than in the other two samples. eGFP3 has the smallest fraction of dark chromophores resulting in the largest $\beta_{HRS,800nm}$ value of 130x10^{-30} esu. Finally, eGFP1 having the intermediate absorption at 400 nm nicely shows an intermediate β hyperpolarizability value at 115x10^{-30} esu.

Comparative assessment of the deconvolution methods

Apart from the excellent numerical agreement between the results obtained from both demodulation techniques in the frequency and in the spectral domain, another comparison should be made in terms of time required for the measurements. HRS has originally been presented as a time-efficient, widely applicable and most convenient measurement technique with respect to, at the time, EFISHG. It does not require the

application of a static electric field and provides a direct measure of the first hyperpolarizability, not convolved with the dipole moment μ as compared to the results from EFISHG always obtained as a $\mu\beta$ value, and the second hyperpolarizability γ. However, when MPF is contributing to the signal, more time is needed to suppress this contribution in the overall signal collected, either in the frequency domain by measuring at multiple AM frequencies or in the spectral domain by measuring at multiple wavelengths. At the time of the first implementations in the spectral domain, a number of discrete measurements at single wavelengths with a photomultiplier tube made this approach time-consuming. Nowadays, with the availability of very sensitive photodiode arrays or CCD cameras, it is possible to measure a quasi-continuous spectrum and apply averaging by simply accumulating over time. This makes the implementation in the spectral domain the preferred technique nowadays. The implementation of the spectral method in microscopy is also much simpler, and is already being used in a simplified way by using a narrow band gap filter at the second harmonic wavelength. However, both MPF and SHG signals are recorded in the same detector channel without discrimination. The simple use of a narrow band-pass filter does not therefore qualify as a method to eliminate the MPF contribution. True MPF elimination requires complete spectral separation from SHG wavelength at which point we lose the advantage of resonance enhancement. Implementation of a fast spectral scanning method may alleviate this problem. With current technological progress, the use of frequency modulated laser beams to eliminate the MPF signal may become viable in the near future as well.

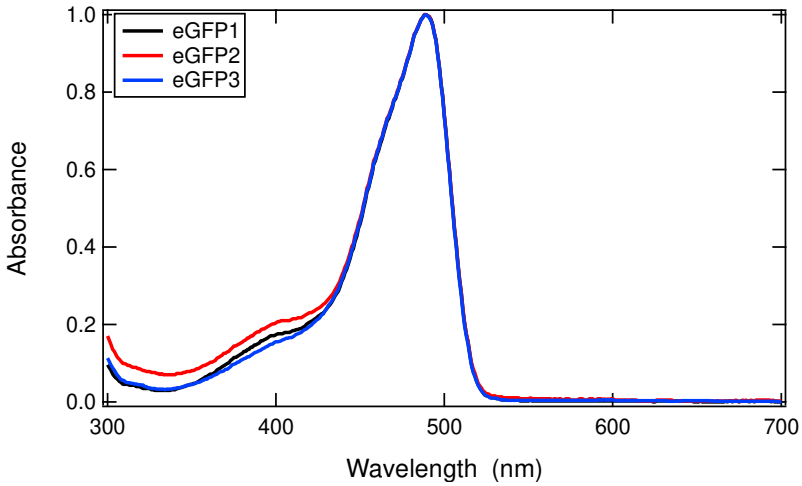

Figure 5. Comparative absorption spectra (normalized to the absorption peak at 488 nm) for eGFP in slightly different buffers, see Table 3, evidencing their effect on the relative contributions from the dark protonated state, absorbing at 400 nm.

As a final note, the approach in the frequency domain appears to have an advantage when MPF is strongly overwhelming the HRS signal. This is a consequence of the active way the fluorescence contribution is not only simply recorded, as in the spectral domain, but actively suppressed by demodulation at higher AM frequencies. And as to the practical aspect of the time needed to measure the signal at multiple discrete harmonics of the fundamental repetition frequency of the pulsed laser, it is possible to use an RF (radio frequency) spectrum analyzer to sweep the RF spectrum, not to be confounded with the wavelength spectrum. The use of an RF spectrum analyzer prohibits, however, the experimental determination of the phase of the signal. As it has been shown that the phase adds substantially to the preciseness as it provides twice the number of experimental data points and to the accuracy as the phase as a function of AM frequency is a very sensitive function of the importance of the MPF contribution, it is felt that this approach towards time efficiency is not going to threaten the approach in the spectral domain as overall, in terms of time needed, accuracy and precision, the current technique of choice for nonlinear optical characterization of the molecules to identify the better chromophores.

In nonlinear microscopy one can experiment with combining the higher inherent $\beta_{HRS,o}$ values of the red-shifted chromophores with longer laser wavelengths to benefit from a stronger inherent signal and resonance enhancement to increase the effectively measured signal. Currently available pulsed lasers are often performing longer wavelengths at lower output power that would counteract the intended signal increase. However, to measure fluorescence-free signal, one should measure at wavelengths outside the MPF spectrum, eliminating any benefit from resonance enhancement as well. Commercial microscopes are commonly available with an array of sensitive GaAsP (Gallium Arsenide Phosphide) detectors to measure full spectra with 7-11 nm spectral resolution in a single scan. The newest (*e.g.* hybrid) detectors being developed for confocal imaging are giving promising results towards spectral resolution and sensitivity. They can perfectly detect SHG signals in an MPF-free background, and future models may be able to discern the signal on top of an MPF signal. Or instead, a specialized detector could be built that measures a narrow bandwidth (*e.g.* 390-410 nm with 1 nm spectral resolution for the commonly used 800 nm laser excitation. This could be combined with the deconvolution method approach in the spectral domain, initially as post measurement analysis but with sufficient processing power eventually as a live imaging algorithm to filter

out MPF and show SHIM images alongside MPF images, potentially even at the same wavelengths. An alternative is the use of chromoproteins that should not have any contribution from fluorescence in the SHG signal. The Channel rhodopsins characterized in this work show a relatively high inherent $\beta_{HRS,o}$ value, and in addition a high $\beta_{HRS,\lambda}$, due to the strong resonance enhancement, both at 800 and at 1064 nm fundamental wavelength because of the absorption maximum of 470 nm in between the second-harmonic wavelengths of 400 and 532 nm. They have the highest apparent $\beta_{HRS,\lambda}$ value compared to all fluorescent proteins in this work, both at 800 and 1064 nm. Channel rhodopsins are membrane proteins and could therefore be excellent probes for nonlinear imaging of membrane potentials and for nonlinear membrane potential determination, but they would not be readily usable for cytoplasmic applications.

Conclusions and perspectives

From a comparative study of the experimental determination of the first hyperpolarizability of a series of fluorescent proteins and one opsin, it is concluded that the two approaches to deal with the multiphoton fluorescence contribution to the hyper-Rayleigh scattering signal, namely in the spectral and in the frequency domain, are equivalent, in terms of accuracy and precision. From the retrieved values for the series of fluorescent proteins, it is confirmed that the longer the conjugated path in the chromophore in the protein inside, the larger the static first hyperpolarizability value ($\beta_{HRS,o}$), resulting in the more red emitting (and absorbing) proteins to be more efficient for SHIM. However, because of the stronger resonance enhancement experienced by the blue absorbing variants with the fundamental wavelength of the omni-present Titanium-sapphire femtosecond pulsed laser, the dynamic $\beta_{HRS,\lambda}$ values, relevant for the experiments, are larger. Besides resonance enhancement, the more subtle influence of the pH on the first hyperpolarizability value for eGFP has also been elucidated. While SHIM is currently making use of filters to select for the second harmonic wavelength, this does not guarantee fluorescence-free signals. The implementation of demodulation in SHIM would preferably use the spectral method, which only needs minor new developments in the detection mechanisms currently in use. The use of chromoproteins would also be a valid alternative for fluorescence-free SHIM, not only for their inherently fluorescence-free response, but also for their large second-order nonlinear response, despite their obligate symmetric, yet not centrosymmetric,

dimeric nature. The sizeable first hyperpolarizability value for the ChR mutants demonstrates to the non-centrosymmetric nature of the dimeric constructs, pointing to their potential for SHIM and membrane potential measurements.

The technological evolution towards using further red-emitting FPs, for the advantages associated with better light propagation and lower energy of longer wavelengths, for deeper penetration, less phototoxicity and better photostability, is nicely mirrored by the technical evolution in laser physics, resulting in the commercial availability of fairly simple, completely computer-controlled and widely tunable, notably more in the near-IR, femtosecond laser sources. This promises a bright future for the use of fluorescent proteins and chromoproteins in applications of their second-order nonlinear optical properties.

Acknowledgements

The authors acknowledge financial support from PHC Egide –Tournesol bilateral program France-Flanders. LV, KC and JH acknowledge support from the Flemish Fund for Scientific Research (FWO-V, G048412N). YdC, CB and KC acknowledge support from the University of Leuven (IDO/12/07). LV acknowledges support from the Flemish Fund for Scientific Research (FWO-V, project number). IRA and PFB acknowledge financial support from the French National Agency for Research (ANR) under project ANR-CE24-2017-0029. We thank Prof. Peter Hegemann and Dr. Katja Stehfest from the Humboldt University of Berlin for providing the *Pichia* cell lines for expression of the Channel Rhodopsin mutants.

EDM current address: Marine Biology Research Division, Scripps Institution of Oceanography, University of California, San Diego, 9500 Gilman Drive, La Jolla, CA 92093-0202, USA

References

[1] Dedecker P., De Schryver F.C., Hofkens J., Fluorescent Proteins: Shine on, You Crazy Diamond, J. Am. Chem. Soc., (2013) 135, 2387-2402.

[2] Shaner N.C., Steinbach P.A., Tsien R.Y., A guide to choosing fluorescent proteins, Nat. Methods, (2005) 2, 905-909.

[3] Sakaue-Sawano A., Kurokawa H., Morimura T., Hanyu A., Hama H., Osawa H., Kashiwagi S., Fukami K., Miyata T., Miyoshi H. Imamura T., Ogawa M., masai H., Miyawaki A., Visualizing spatiotemporal dynamics of multicellular cell-cycle progression, Cell (2008) 132, 487-498.

[4] Livet J., Weissman T.A., Kang H.N., Draft R.W., Lu J., Bennis R.A., Sanes J.R., Lichtman J.W., Transgenic strategies for combinatorial expression of fluorescent proteins in the nervous system, Nature, (2007) 450, 56-62.

[5] Hoffman R.M., Use of fluorescent proteins and color-coded imaging to visualize cancer cells with different genetic properties, Cancer Metast. Rev., (2016) 35, 5-19.

[6] Reeve J.E., Anderson H.L., Clays K., Dyes for biological second harmonic generation imaging, Phys. Chem. Chem. Phys. (2010) 12, 13484-13498.

[7] Dempsey W.P., Fraser S.E., Pantazis P., SHG nanoprobes: Advancing harmonic imaging in biology, Bioessays (2012) 34, 351–360

[8] Khatchatouriants A., Lewis A., Rothman Z., Loew L., Treinin M., GFP is a selective non-linear optical sensor of electrophysiological processes in Caenorhabditis elegans, Biophys. J., (2000) 79, 2345-2352.

[9] Lewis A., Khatchatouriants A., Treinin M., Chen Z.P., Peleg G., Friedman N., Bouevitch O., Rothman Z., Loew L;, Sheres M., Second-harmonic generation of biological interfaces: probing the membrane protein bacteriorhodopsin and imaging membrane potential around GFP molecules at specific sites in neuronal cells of C. elegans, Chem. Phys., (1999) 245, 133-144.

[10] Jiang J., Eisenthal K.B., Yuste R., Second harmonic generation in neurons: electro-optic mechanism of membrane potential sensitivity, Biophys J. (2007) 93, L26-L28.

[11] Reeve J.E., Corbett A.D., Boczarow I., Kaluza W., Barford W., Bayley H., Wilson T., Anderson H.L., Porphyrins for Probing Electrical Potential Across Lipid Bilayer Membranes by Second Harmonic Generation, Angew. Chem. Int. Ed. (2013) 52, 9044-9048.

[12] Asselberghs I., Flors C., Ferrighi L., Botek E., Champagne B., Mizuno H., Ando R., Miyawaki A., Hofkens J., Van der Auweraer M., Clays K., Second-Harmonic Generation in GFP-like Proteins, J. Am. Chem. Soc. (2008) 130, 15713-15719.

[13] De Meulenaere E., Asselberghs I., de Wergifosse M., Botek E., Spaepen S., Champagne B., vanderleyen J., Clays K., Second-order nonlinear optical properties of fluorescent proteins for second-harmonic imaging, J. Mater. Chem. (2009) 19, 7514-7519.

[14] De Meulenaere E., De Wergifosse M., Botek E., Spaepen S., Champagne B., Vanderleyden J., Clays K., Nonlinear Optical Properties of Mstrawberry and Mcherry for Second Harmonic Imaging, J. Nonlin. Opt. Phys. Mat. (2010) 19, 1-13.

[15] De Meulenaere E., Nguyen Bich N., de Wergifosse M., Van Hecke K., Van Meervelt L., Vanderleyden J., Champagne B., Clays K., Improving the second-order nonlinear optical response of fluorescent proteins: the symmetry argument, J. Am. Chem. Soc. (2013) 135, 4061-4069.

[16] Birge R.R., Fleitz P.A., Lawrence A.F., Masthay M.A., Zhang C.F., Nonlinear Optical-Properties of Bacteriorhodopsin - Assignement of 2nd-Order Hyperpolarizabilities of Randomly Oriented Systems Using Two-Photon Spectroscopy, Mol. Cryst. Liq. Cryst. (1990) 189, 107-122.

[17] Birge R.R., Zhang C.F., Two-Photon Double-Resonance Spectroscopy of Bacteriorhodopsin - Assignment of the Electronic and Dipolar Properties of the Low-Lying $^1A_g{}^{*-}$-Like and $^1B^-{}_u$-$^{*+}$-Like π,π^* States, J. Chem. Phys. (1990) 92, 7179-7195.

[18] Boyden E.S., Zhang F., Bamberg E., Nagel G., Deisseroth K., Millisecond- timescale genetically targeted optical control of neural activity, Nat. Neurosci. (2005) 8, 1263–1268.

[19] Deisseroth K., Optogenetics: 10 years of microbial opsins in neuroscience, Nat. Neurosci. (2005) 18, 1213–1225.

[20] Clays K., Hendrickx E., Triest M., Verbiest T., Persoons A., Dehu C., Brédas J.L. Nonlinear-Optical Properties of Proteins Measured by Hyper-Rayleigh Scattering in Solution, Science (1993) 262, 1419-1422.

[21] Rekas A., Alattia J.R., Nagai T., Miyawaki A., Ikura M., Crystal structure of Venus, a yellow fluorescent protein with improved maturation and reduced environmental sensitivity, J. Biol. Chem. (2002) 277, 50573-50578.

[22] Remington S.J., Wachter R.M., Yarbrough D.K., Branchaud B., Anderson D.C., Kallio K., Lukyanov K.A., zFP538, a yellow-fluorescent protein from Zoanthus, contains a novel three-ring chromophore, Biochem. (2005) 44, 202-212.

[23] Filonov G.S., Piatkevich K.D., Ting L.M., Zhang J.H., Kim K., Verkhusha V.V., Bright and stable near-infrared fluorescent protein for in vivo imaging, Nat. Biotechnol. (2011) 29, 757-761.

[24] Lin, J.Y., Lin M.Z., Steinbach P., Tsien R.Y., Characterization of Engineered Channelrhodopsin Variants with Improved Properties and Kinetics, Biophys. J. (2009) 96, 1803-1814.

[25] McIsaac R.S., Bedbrook C.N., Arnold F.H., Recent advances in engineering microbial rhodopsins for optogenetics, Curr. Opin. Struct. Biol. (2015) 33, 8–15.

[26] Wietek J., Wiegert J.S., Adeishvili N., Schneider F., Watanabe H., Tsunoda S.P., Vogt A., Elstner M., Oertner T. G., Hegemann P., Conversion of channelrhodopsin into a light-gated chloride channel, Science (2014) 344, 409–412.

[27] Berndt A., Schoenenberger P., Mattis J., Tye K.M., Deisseroth K., Hegemann P., Oertner T.G., High-efficiency channelrhodopsins for fast neuronal stimulation at low light levels, Proc. Nat. Acad. Sci. (2011) 108, 7595–600.

[28] Ritter E., Piwowarski P., Hegemann P., Bartl F.J., Light-dark Adaptation of Channelrhodopsin C128T Mutant, J. Biol. Chem. (2013) 288, 10451-10458.

[29] Yizhar O., Fenno L.E., Prigge M., Schneider F., Davidson T.J., O'Shea D.J., Sohal V.S., Goshen I., Finkelstein J., Paz J.T., Stehfest K., Fudim R., Ramakrishnan C., Huguenard J.R., Hegemann P., Deisseroth K., Neocortical excitation/inhibition balance in information processing and social dysfunction, Nature (2011) 477, 171–178.

[30] Noordman O.F.J., van Hulst N.F., Time-resolved hyper-Rayleigh scattering: Measuring first hyperpolarizabilities beta of fluorescent molecules, Chem. Phys. Lett. (1996) 253, 145-150.

[31] Clays K., Wostyn K., Olbrechts G., Persoons A., Watanabe A., Nogi K., Duan X.M., Okada S., Oikawa H., Nakanishi H., Vogel H., Beljonne D., Brédas J.L., Fourier analysis of the femtosecond hyper-Rayleigh scattering signal from ionic fluorescent hemicyanine dyes, J. Opt. Soc. Am. B (2000) 17, 256-265.

[32] Olbrechts G., Strobbe R., Clays K., Persoons A., High-frequency demodulation of multi-photon fluorescence in hyper-Rayleigh scattering, Rev. Sci. Instrum. (1998) 69, 2233-2241.

[33] Olbrechts G., Wostyn K., Clays K., Persoons A., High-frequency demodulation of multiphoton fluorescence in long-wavelength hyper-Rayleigh scattering, Opt. Lett. (1999) 24, 403-405.

[34] Hubbard S.F., Petschek R.G., Singer K.D., Spectral content and dispersion of hyper-Rayleigh scattering, Opt. Lett. (1996) 21, 1774-1776.

[35] Duboisset J., Matar G., Russier-Antoine I., Benichou E., Bachelier G., Jonin Ch., Ficheux D., Besson F., P.F. Brevet, First Hyperpolarizability of the Natural Aromatic Amino Acids Tryptophan, Tyrosine, and Phenylalanine and the Tripeptide Lysine-Tryptophan-Lysine Determined by Hyper-Rayleigh Scattering, J. Phys. Chem. B (2010) 114, 13861–13865.

[36] Hsu C.C., Huang T.H., Zang Y.L., Lin J.L., Cheng Y.Y., Lin J.T., Wu H.H., Hyperpolarizabilities of the m-substituent phenyl amine based chromophores determined from the hyper-Rayleigh scattering and two photon absorption induced fluorescence, J. Appl. Phys. (1996) 80, 5996-6001.

[37] Campo J., Desmet F., Wenseleers W., Goovaerts E., Highly sensitive setup for tunable wavelength hyper-Rayleigh scattering with parallel detection and calibration data for various solvents, Opt. Express (2009) 17, 4587-4604.

[38] de Coene Y, Van Cleuvenbergen S, Van Steerteghem N, Baekelandt V, Verbiest T, Bartic C, Clays K., Fluorescence-Free Spectral Dispersion of the Molecular First Hyperpolarizability of Bacteriorhodopsin, J. Phys. Chem. C (2017) 121, 6909-6915.

[39] Nappa J., Revillod G., Abid J.P., Russier-Antoine I., Jonin C., Benichou E., Girault H.H., Brevet P.F., Hyper-Rayleigh scattering of gold nanorods and their relationship with linear assemblies of gold nanospheres, Faraday Disc. (2004) 125, 145-156.

[40] Russier-Antoine I., Jonin C., Nappa J., Benichou E., Brevet P.F., Wavelength dependence of the hyper Rayleigh scattering response from gold nanoparticles, J. Chem. Phys. (2004) 120, 10748-10752.

[41] Tomosugi W., Matsuda T., Tani T., Nemoto T., Kotera I., Saito K., Horikawa K., Nagai T., An ultramarine fluorescent protein with increased photostability and pH insensitivity, Nat. Methods (2009) 6, 351-353.

[42] Verbiest T., Clays K., Persoons A., Meyers F., Bredas J.L., Determination of the Hyperpolarizabilitiy of an Octopolar Molecular Ion by Hyper Rayleigh Scattering, Opt. Lett. (1993) 18, 525-527.

[43] Brasselet S., Zyss. J., Multipolar molecules and multipolar fields: probing and controlling the tensorial nature of nonlinear molecular media, J. Opt. Soc. Am. B (1998) 15, 257 - 288.

[44] Revillod G., Duboisset J., Russier-Antoine I., Benichou E., Bachelier G., Jonin C., Brevet P.F., Multipolar contributions to the second harmonic response from mixed DiA-SDS molecular aggregates, J. Phys. Chem. C (2008) 112, 2716-2723.

[45] Hemmer E., Benayas A., Légaré F., Vetrone F., Exploiting the biological windows: current perspectives on fluorescent bioprobes emitting above 1000 nm, Nanoscale Horiz., (2016) 1, 168-184

[46] Miao Y., Gu C., Zhu Y., Yu B., Shen Y., Cong H., Recent Progress in Fluorescence Imaging of the Near‐Infrared II Window, ChemBioChem (2018) 19, 2522 – 2541

[47] Shcherbakova D.M., Baloban M., Verkhusha V.V, Near-infrared fluorescent proteins engineered from bacterial phytochromes, Curr. Opin. Chem. Biol. (2015) 27: 52–63.

[48] Haupts U., Maiti S., Schwille P., Webb W.W., Dynamics of fluorescence fluctuations in green fluorescent protein observed by fluorescence correlation spectroscopy, Proc. Nat. Acad. Sci. (1998) 95, 13573-13578.